Journal of Low Temperature Physics
https://doi.org/10.1007/s10909-024-03171-5

Majorana Modes and Fano Resonances in Aharonov–Bohm Ring with Topologically Nontrivial Superconducting Bridge

S. V. Aksenov[1] · **M. Yu. Kagan**[2,3]

Received: 1 March 2024 / Accepted: 3 June 2024

Abstract
We study different resonances (first of all of the Fano type) in the interference device formed by the Aharonov–Bohm ring with superconducting (SC) wire in the topologically nontrivial state playing a role of a bridge between top and bottom arms. We analyze Majorana modes on the ends of the SC wire and show that the collapse of the additional Fano resonance, that is initially induced by transport scheme asymmetry, is connected with the increase of the length of the bridge when the binding energy of the Majorana end modes tends to zero. In local transport regime, the Fano resonances are stable against the change of the transport symmetry. The reasons of both collapse and sustainability are analyzed using a spinless toy model including the Kitaev chain.

Keywords Topological superconductivity · Majorana modes · Aharonov–Bohm ring · Fano resonanse

1 Introduction

The subject of the topological superconductivity and Majorana [1] modes is very fashionable nowadays. In topological superconductors there are Majorana bound states which are formed by the pair of the Majorana modes. These states are

✉ S. V. Aksenov
asv86@iph.krasn.ru

M. Yu. Kagan
mkagan@hse.ru

[1] Kirensky Institute of Physics, Siberian Branch of Russian Academy of Sciences, Akademgorodok 50/38, Krasnoyarsk, Russia 660036

[2] National Research University Higher School of Economics, Myasnitskaya Street 20, Moscow, Russia 101000

[3] P.L. Kapitza Institute for Physical Problems, Russian Academy of Sciences, Kosygin Street 2, Moscow, Russia 119334

Published online: 15 June 2024

characterized by the spatial nonlocality, quantum entanglement and nonabelian statistics. These features define the interest to topological superconductors and topologically protected qubits based on them [2].

The necessary condition for the realization of the topological insulator state as we know is a presence of a band structure with band inversion and spin-orbit coupling. For some topological superconductors with Majorana modes an important ingredient is the SC pairing of electrons with the same spin projection, i.e. triplet pairing. (see e.g. [3, 4] for the review)

We note that the concept of topological superconductivity was closely connected historically with the earlier studies of the triplet p-wave superfluidity and the symmetry of the order parameter in the A- and B-phases of the superfluid He-3.

Let us emphasize that in several tunneling spectroscopy experiments with InAs and InSb SW (exhibiting strong spin-orbit coupling and induced SC pairing) we get some support in favor of the formation of the MBS (see [18, 21]). However, the decisive evidence is still lacking and cannot be connected just with the quantization of the conductance at zero voltage [22, 23]. That is why more profound approaches probing other features of the MBS, e.g. its spatial nonlocality or spin polarization, should be considered [24]. One of these approaches can be based on the investigation of the Fano resonances in the Aharonov-Bohm (AB) ring with the SW playing a role of bridge that is considered further.

In this article we will study the Majorana modes and the appearance and collapse of the Fano resonances in the Aharonov–Bohm ring with the SC bridge. We will consider the superconducting bridge, which can be transferred in topologically nontrivial phase, between lower and upper shoulders of the Aharonov–Bohm ring [5] (see Fig. 1 and [4, 6, 7]). Note that in the geometry of Fig. 1 we have an interference device suitable to study the effects of the Aharonov–Bohm phase, different resonances (the Fano and Breit-Wigner type [8, 9]) and topologically nontrivial excitations such as Majorana bound states. To be more specific on Fig. 1 of this section we consider a SC bridge in an s-wave state in the presence of Rashba spin-orbit coupling [10, 11] and the in-plane magnetic field in the Aharonov–Bohm ring. The

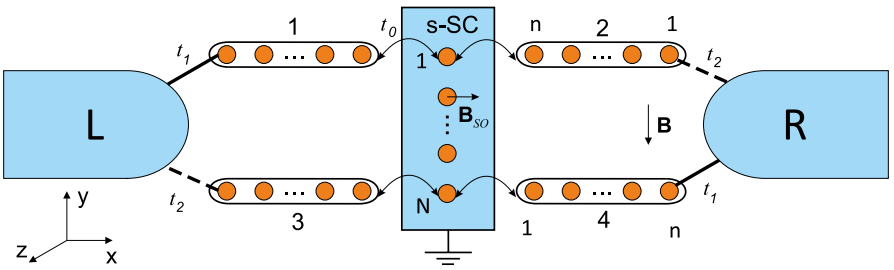

Fig. 1 The superconducting nanowire (s-wave SC with Rashba spin-orbit coupling) including N sites and connecting the shoulders (the arms) of the Aharonov–Bohm ring or an interference device formed by four leads (each with n sites): 1-left top (LT) and 2-right top (RT) on the upper shoulder; 3- left bottom (LB) and 4-right bottom (RB) on the lower shoulder. The shoulders are in the normal state (NW) and their ends are connected in parallel with metallic contacts L, R. We show on the Fig. the hopping integrals t_0, t_1, t_2, external magnetic field $\mathbf{B}$ and effective Rashba field $\mathbf{B}_{so}$

Aharonov–Bohm ring in this scheme is an interference device formed by four leads: 1-left top (LT) and 2-right top (RT) on the upper shoulder; 3-left bottom (LB) and 4-right bottom (RB) on the lower shoulder. The shoulders are in the normal state, i.e. the leads are normal wires (NWs), and their ends are connected in parallel with metallic contacts.

This interference device contains a very rich physics connected first of all with the Majorana modes in the superconducting wire (SW). We will show that some effects of spinful coherent transport can be described by the spinless toy model including 4 normal sites located of the sides of the Kitaev chain [12] with even number of sites ($N = 2$ and $N = 4, 6, ...$) in (see [7] and Figs. 2a and b).

Qualitatively, the appearance and collapse of the different resonances in this scheme can be explained by the presence of two interacting transport channels in the system. As a result, the Fano resonances are connected with the bound states in the continuum (BICs). We will show that the width and the position of these resonances is highly sensitive to the lowest in energy excitations in the SW, which in topologically nontrivial phase corresponds to Majorana bound states (MBS) or Andreev bound states [13, 14]. This study is mostly focused on an asymmetric transport regime featured by different hopping integrals t_1 and t_2. These quantities describe the tunnel processes between the left (right) contact and the LT (RB) and LB (RT) leads, respectively. Note that the Fano effect in the similar geometry was analyzed in [15]. However, its authors considered the symmetric transport regime and did not observe the disappearance of the Fano resonances due to the MBS nonlocality.

2 Topological Superconductivity in 1D Nanostructures

In this section we provide a brief introduction to the subject of topological superconductivity in 1D nanostructures. Note that the topological superconductivity is a very fashionable field of research nowadays because of its importance for the protection of the phase in the superconducting qubits under the external perturbations. The

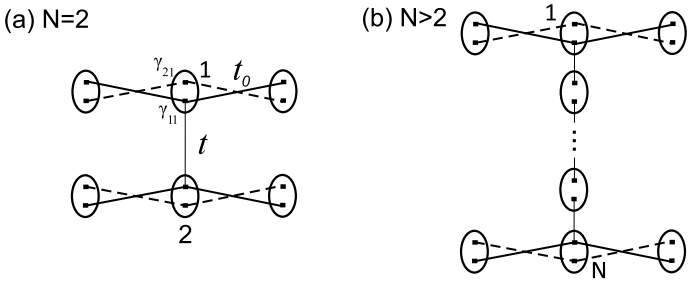

Fig. 2 The Aharonov–Bohm ring with $n = 1$ for each normal wire and the superconducting bridge described by Kitaev chain with $N = 2$ **a** or larger even number of sites $N = 4, 6, ...$ **b**. The dots inside the ellipses denote the Majorana operators of the 1st and 2nd type in real space, γ_{1j} and γ_{2j}, respectively

manifestation of the nontrivial topology in 1D structures such as SW first of all is connected with the presence of the MBSs.

As we mentioned already, the basic scenario for the formation of the MBS in the 1D system is connected with the combination of three factors: SC pairing, spin-orbit coupling and an external magnetic field [16, 17]. Often this situation is realized for the NW on the surface of the massive s-wave SC [18]. In this case the topological superconductivity in the NW is induced by the proximity effect.

In the geometry of Fig. 1, when $\mathbf{B} \perp \mathbf{B}_{so}$ two sub-bands arise in the normal state of the bridge with a gap at $k = 0$ that is equal to a Zeeman energy h (where k—wave vector). If a chemical potential μ is in the gap center that the SC pairing between the electrons of the same sub-band dominates. Thus, effectively in this case the pairing of electrons in SW is equivalent to the triplet p-wave pairing [19] that was initially considered in the spinless Kitaev model [12].

This type of the pairing with $l = S = 1$ takes place, e.g. in the superfluid He-3. Generally, in the absence of the field there are three components of the magnetic quantum number $m = l_z$ and three components of the spin-projection S_z in the isotropic B-phase of He-3. However, in strong magnetic fields the anisotropic triplet A-phase is realized with the pairing of two up spins on larger Fermi surface and two down spins on the smaller one, similar to the pairing of electrons on the same sub-band in the SW.

Note that the importance of the spin-orbit coupling can be understood more formally as well. It is necessary for the appearance of the self-conjugated Bogoliubov operators $\beta_0 = \beta_0^+$ describing the Majorana quasi-particles in the more realistic situation when electrons have spin degrees of freedom. The fulfillment of this condition requires the strong mixing of up and down spin projections of electrons in the Bogoliubov u-v representation. Thus, the appealing typical representation of the BCS-type, where $\beta_0 \sim u_j a_{j\uparrow} + v_j a_{j\downarrow}^+$, is forbidden [3].

3 Kitaev Chain Model

In the Kitaev model [12] the emergence of the MBS was demonstrated at $2t > |\mu|$ and $\Delta \neq 0$, where t—a hopping integral for electron between the neighboring sites of the chain; Δ—an SC gap. In the specific case of

$$|\Delta| = t, \ \mu = 0, \tag{1}$$

the MMs arise only on the first and last sites of the chain.

To be more specific we consider the 1D Hamiltonian of Kitaev chain with N sites:

$$\hat{H} = -\mu \sum_{j=1}^{N} \left(a_j^+ a_j - \frac{1}{2} \right) - \sum_{j=1}^{N-1} \left(t a_j^+ a_{j+1} - \Delta a_j^+ a_{j+1}^+ + h.c. \right), \tag{2}$$

where a_j^+ and a_{j+1} are the creation and annihilation operators of spinless fermions on sites j and $j + 1$, respectively. The SC order parameter is

$$\Delta = |\Delta| e^{i\Theta} \tag{3}$$

and Θ is the phase of the order parameter which is assumed to be fixed.

After that we can perform the transformation from fermionic operators a_j^+ and a_j to Majorana self-conjugated operators γ_{1j} and γ_{2j} according to the prescription:

$$\begin{aligned} \gamma_{1j} =& e^{\frac{i\Theta}{2}} a_j + e^{-\frac{i\Theta}{2}} a_j^+, \\ \gamma_{2j} =& -ie^{\frac{i\Theta}{2}} a_j + ie^{-\frac{i\Theta}{2}} a_j^+, \end{aligned} \tag{4}$$

It is easy to understand from the expressions (4) that indeed:

$$\gamma_{1,2j} = \gamma_{1,2j}^+ \tag{5}$$

Correspondingly for the anti-commutators of Majorana operators on the same site we get the relations:

$$\{\gamma_{1,2j}, \gamma_{1,2j}\} = 2 \tag{6}$$

while for the operators on the neighboring sites:

$$\{\gamma_{\alpha j}, \gamma_{\beta j+1}\} = 0, \quad \alpha,\ \beta = 1, 2. \tag{7}$$

Thus, from the Eq. (6) we can see the striking difference between the anti-commutation relations of fermions and Majoranas on the same site.

Besides that, the Majorana modes have exactly zero energies. To show that, by analogy with the real-space representation via the Majorana operators discussed above, one can perform the same procedure for the Bogoliubov operators. In particular, for the lowest-energy excitation (possessing an index '0') we can write $\beta_0 = \left(b_1 + ib_2\right)/2$. Indeed, as it was noticed by Bogoliubov, we should satisfy two equations of motion simultaneously: $i\dot{b}_{1,2} = \varepsilon_0 b_{1,2}$ and $i\dot{b}_{1,2}^+ = -\varepsilon_0 b_{1,2}^+$ for Majorana operators $b_{1,2}$ and $b_{1,2}^+$. But, since $b_{1,2} = b_{1,2}^+$, we have to assume that $\varepsilon_0 = -\varepsilon_0$, and hence, $\varepsilon_0 = 0$.

Moreover, we can rewrite the Hamiltonian in Eq. (2) in terms of Majorana operators as follows:

$$\hat{H} = -\frac{i}{2}\mu \sum_{j=1}^{N} \gamma_{1j}\gamma_{2j} + \frac{i}{2} \sum_{j=1}^{N-1} \left[(t + |\Delta|)\gamma_{2j}\gamma_{1j+1} + (-t + |\Delta|)\gamma_{1j}\gamma_{2j+1}\right]. \tag{8}$$

If we consider a special point in the parameter space where $|\Delta| = t$ and $\mu = 0$, then a simple form of the Hamiltonian expressed only via Majorana operators on the neighboring sites appears,

$$\hat{H} = it \sum_{j=1}^{N-1} \gamma_{2j}\gamma_{1j+1}. \tag{9}$$

Now it is convenient to perform the inverse transformation from Majorana operators γ_{1j+1} and γ_{2j} in Eq. (9) to the new fermionic nonlocal operators $\tilde{a}_j$ and $\tilde{a}_j^+$ assuming that they satisfy the relations:

$$\begin{aligned} \gamma_{2j} =& \tilde{a}_j + \tilde{a}_j^+, \\ \gamma_{1j+1} =& -i\tilde{a}_j + i\tilde{a}_j^+, \quad j = 1, 2, ..., N-1. \end{aligned} \tag{10}$$

We can resolve the Eq. (10) and get the representation for the new operators $\tilde{a}_j$ and $\tilde{a}_j^+$ via the Majorana operators γ_{1j+1} and γ_{2j}. This yields:

$$\begin{aligned} \tilde{a}_j =& \big(\gamma_{2j} + i\gamma_{1j+1}\big)/2, \\ \tilde{a}_j^+ =& \big(\gamma_{2j} - i\gamma_{1j+1}\big)/2, \quad j = 1, 2, ..., N-1. \end{aligned} \tag{11}$$

Then we can easily express the product of Majorana operators $\gamma_{2j}\gamma_{1j+1}$ via the fermionic one:

$$\gamma_{2j}\gamma_{1j+1} = \frac{2}{i}\Big(\tilde{a}_j^+\tilde{a}_j - \frac{1}{2}\Big). \tag{12}$$

and, finally, diagonalize the Hamiltonian of the Kitaev chain in the real space:

$$\hat{H} = 2t\sum_{j=1}^{N-1}\Big(\tilde{a}_j^+\tilde{a}_j - \frac{1}{2}\Big). \tag{13}$$

Note that from Eq. (11) we can see that the operators $\tilde{a}_j$ and $\tilde{a}_j^+$ satisfy indeed the usual fermionic anti-commutation relations:

$$\{\tilde{a}_j, \tilde{a}_j\} = \{\tilde{a}_j^+, \tilde{a}_j^+\} = 0, \ \{\tilde{a}_j, \tilde{a}_j^+\} = 1. \tag{14}$$

However, there is one important point in the Hamiltonian (13), namely the index j covers $N-1$ instead of N values. In other words, some degrees of freedom are missing in the Eq. (13). They correspond to Majorana massless fermions. At the same time in the Eq. (9), where the Hamiltonian is expressed in terms of Majorana operators, the two operators on the ends of the chain γ_{11} and γ_{2N} are also absent. Hence the ground state is doubly degenerate. It means [20] that a product of these missing operators

$$i\gamma_{11}\gamma_{2N} = \pm 1, \tag{15}$$

while the other products which enter in the Hamiltonian (9) are single valued:

$$i\gamma_{2j}\gamma_{1j+1} = 1, \quad 1 \le j \le N-1. \tag{16}$$

The operators γ_{11} and γ_{2N} describe the zero energy Majorana modes.

Note that the two states in (15) with $i\gamma_{11}\gamma_{2N} = \pm 1$ are practically indistinguishable. They can be distinguished only by the parity operator which is nonlocal. Indeed, an operator which distinguish these states should act simultaneously on both end

sites 1 and N and thus it cannot be local. Hence these end states form a qubit. Moreover, from Eqs. (9)–(16) we observe that the qubit states are topologically protected because they are separated from the excited states by a gap $|\Delta| = t$ and immune to the local perturbations due to the MBS nonlocality in space on the length of the chain L.

If we go away from the special point, where $|\Delta| = t$, we get the similar physical picture. There is a gap above the two nearly degenerate ground states with opposite parity. The MBS energy splits from zero value due to the overlap of their MM Ψ -functions on the chain of the finite length. We can say, that such a hybridization yields the binding energy for the Majorana end states which is proportional to:

$$E_b \sim \exp\left(-\frac{L}{\xi_0}\right) \to 0 \text{ for } N \to \infty. \tag{17}$$

and is exponentially decreasing with the increase of the length of the chain $L = (N-1)d$, where d is the inter-site distance. In Eq. (17) the coherence length enters,

$$\xi_0 \sim \frac{\hbar v_F}{|\Delta|}, \tag{18}$$

which is inversely proportional to the absolute value of the gap. Note that the expression (17) for the energy of the MBS persists even in more physically relevant region, where $|\Delta| < t$.

Note that the nontrivial topology in the Kitaev chain is defined by the so-called Majorana number:

$$M = \text{sign}\left(\mu^2 - 4t^2\right). \tag{19}$$

Topologically nontrivial phase in Eq. (19) is related to the value of $M = -1$ of the Majorana number. This situation is realized for the chemical potentials lying inside the band, $-2t < \mu < 2t$. It is essential that a gap of a bulk spectrum $\varepsilon_k = \sqrt{(\mu + 2t\cos k)^2 + 4\Delta^2 \sin^2 k}$ closes and reopens at $\mu = 2t$ and a symmetric nodal point $\bar{k} = \pi$ or $\mu = -2t$ and $\bar{k} = 0$, i.e., on the borders of the topologically trivial and nontrivial regions. The latter indicates that topological phase transition is quantum phase transition.

Note that often in the problems of mesoscopic superconductivity the chains with odd and even number of sites yield the different results with respect to total energy. In the absence of Majorana end modes their difference in energy is just the energy cost of a single unpaired electron on the chain with odd number of sites. Thus $E_{\text{odd}}(2N+1) > E_{\text{even}}(2N)$. The appearance of the Majorana zero energy modes on the two ends of Kitaev chain eliminate this difference between odd and even number of sites [20], and hence:

$$E_{\text{odd}}(2N+1) = E_{\text{even}}(2N). \tag{20}$$

Note also that the distribution of the Bogoliubov u-v coefficients over the different sites $j = 1, 2, ..., N.$ in the normalization condition $\sum_{j=1}^{N}[|u_j|^2 + |v_j|^2] = 1$ also changes drastically when we work inside the region of topologically nontrivial phase. Namely, for $\mu = 0$ and $|\Delta| = t$ the combination $|u_j|^2 + |v_j|^2$ (which enters in the normalization condition) for the long chains have two explicit maxima at the two ends of the chain for $j = 1$ and $j = N$. For both maxima

$$u_1 = v_1 = u_N = -v_N = 1/2, \tag{21}$$

and thus:

$$|u_j|^2 + |v_j|^2 = 0 \, for \, j \neq 1, N. \tag{22}$$

In the same time for $\mu = -2t$ on the border of the topological interval the combination

$$|u_j|^2 + |v_j|^2 \to 1/N \tag{23}$$

is distributed almost in a uniform way between all the sites of the chain including its both ends.

4 Hamiltonian of the Anisotropic Aharonov–Bohm Ring with Superconducting Bridge

In this section we study anisotropic AB ring with different hopping integrals $t_1 \neq t_2$ between the contacts and the shoulders of the device on Fig. 1. Left contact (L) has the hopping integral t_1 with upper shoulder and t_2 with the lower one. For the right contact (R)the situation is opposite: t_1 with lower shoulder and t_2 with the upper one. We will show that in the anisotropic situation new Fano resonances appear in the conductance of the ring [7]. Moreover, the width of these resonances is connected with the degree of the nonlocality of the lowest energy state of the SW.

In other words, the width is governed by the MBS energy whose deviation from zero arises due to the overlap of MMs Ψ-functions. If this overlap disappears and the binding energy $E_b \to 0$, then the two Majorana zero modes (two Majorana 'fermions') become noninteracting and the width of the Fano resonance tends to zero. According to [7] in this case we have a collapse of the Fano resonance caused by the MBS nonlocality.

4.1 Hamiltonian of Superconducting Wire

The Hamiltonian of the SW which includes both SC pairing, spin-orbit coupling and the effect of the Zeeman splitting due to the presence of the external magnetic field reads:

$$\hat{H}_{SW} = \sum_{j=1}^{N} \left[\sum_{\sigma} \xi a_{j\sigma}^{+} a_{j\sigma} + \left(\Delta a_{j\uparrow}^{+} a_{j\downarrow}^{+} + iha_{j\uparrow}^{+} a_{j\downarrow} + h.c. \right) \right] + \frac{1}{2} \sum_{\sigma;j=1}^{N-1} \left[-ta_{j\sigma}^{+} a_{j+1,\sigma} + i\alpha\sigma a_{j\bar{\sigma}}^{+} a_{j+1,\sigma} + h.c. \right], \tag{24}$$

where $\xi = \epsilon_d - \mu$ is the onsite energy, ϵ_d is the gate voltage, μ is the chemical potential, t is the nearest neighbors hopping integral in SW, α is Rashba constant for the spin-orbit coupling, Δ is an s-wave SC order parameter,and h is the Zeeman energy related to the magnetic field $\mathbf{B}$ lying in the plane of the interference device.

Then the topologically nontrivial phase is realized when the following inequalities are satisfied [16, 17]:

$$(\xi - t)^2 + \Delta^2 < h^2 < (\xi + t)^2 + \Delta^2. \tag{25}$$

Let us emphasize that Rashba constant α formally does not enter in the inequalities in Eq. (25). However, the nonzero spin-orbit coupling is essential for the formation of the MBS. Moreover, the effective Rashba field $\mathbf{B}_{\text{so}}$ should be perpendicular to the external magnetic field $\mathbf{B}$.

In the forthcoming sections we will scale all the energy parameters in the units of t assuming that $t = 1$, $\mu = 0$, $\Delta = 0.25$, $\alpha = 0.2$.

4.2 Full System Hamiltonian

Note that the upper and lower shoulders of the AB ring and their four leads: left top (LT), left bottom (LB) and right top (RT), right bottom (RB) are in the normal state. In other words, they correspond to the normal nanowires (NWs) and we consider them to be identical. Their Hamiltonians $\hat{H}_{\text{NW}(1-4)}$ can be obtained from Eq. (24) by putting $\Delta = \alpha = 0$ and replacing $a_{j\sigma}$ by $b_{L(R)j\sigma}$ for $\hat{H}_{\text{NW}(1,2)}$ and by $d_{L(R)j\sigma}$ for $\hat{H}_{\text{NW}(3,4)}$.

Finally, the coupling between SW and NW is governed by the tunneling Hamiltonian:

$$\hat{H}_T = -t_0 \sum_{\sigma} \left[\left(b_{Ln\sigma}^{+} + b_{Rn\sigma}^{+} \right) a_{1\sigma} + \left(d_{L1\sigma}^{+} + d_{R1\sigma}^{+} \right) a_{N\sigma} \right] + h.c., \tag{26}$$

where t_0 is the hopping integral between the edge sites of the SW and NW.

In the same time the coupling between the device (which consists of SW+NW) and the contacts is also described by the tunneling Hamiltonian. But now this Hamiltonian plays the role of the interaction operator in the Keldysh diagram technique [25]. It is given by:

$$\hat{V} = -\sum_{k\sigma} \left[c_{Lk\sigma}^{+} \left(t_1 b_{L1\sigma} + t_2 d_{Ln\sigma} \right) + c_{Rk\sigma}^{+} \left(t_2 b_{R1\sigma} + t_1 d_{Rn\sigma} \right) \right] + h.c., \tag{27}$$

where $c^{+}_{L(R)k\sigma}$ is the creation operator for the electron with wave vector k and spin projection σ at the left (right) contact, whereas t_1 and t_2 are the hopping integrals between the contacts and the device.

Note that the Hamiltonians of the left (right) contact have the simple form:

$$\hat{H}_{L(R)} = \sum_{k} \left(\epsilon_k - \mu_{L(R)}\right) c^{+}_{L(R)k\sigma} c_{L(R)k\sigma}, \tag{28}$$

where

$$\mu_{L(R)} = \mu \pm eV/2, \tag{29}$$

is the electro-chemical potential of the left (right) contact which includes the bias voltage eV.

5 Evaluation of Steady-State Current in Keldysh-Nambu Formalism

In this section we present the convenient modified Nambu [26]—Keldysh formalism [25] for the calculation of the steady current of our system (see [4, 6, 7]) in the tight-binding approximation.

We can generalize the Keldysh formalism on the calculation of the steady state current in superconducting state working in Nambu representation. Namely, it is convenient to diagonalize the full Hamiltonian of the device

$$\hat{H}_D = \hat{H}_{\mathrm{SW}} + \sum_{i=1}^{4} \hat{H}_{\mathrm{NW},i} + \hat{H}_T, \tag{30}$$

utilizing the Nambu operators [26] in the site representation:

$$\hat{f}_j = \left(f_{j\uparrow}\, f^{+}_{j\downarrow}\, f_{j\downarrow}\, f^{+}_{j\uparrow}\right)^{T}, \tag{31}$$

where $f_{j\sigma}$ is the annihilation operator of an electron with spin projection σ at the j-th site of the SW or NW. Then we can define the matrix Keldysh Green's function [7] of the AB ring in the following form:

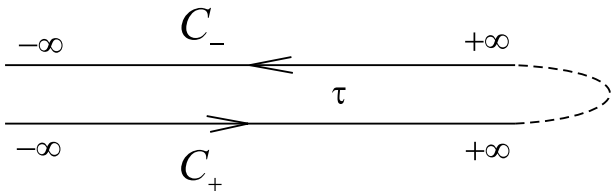

Fig. 3 Keldysh time contour C with the lower branch C_- and the upper branch C_+. The time τ_- on the contour is always 'after' the time τ_+

$$\hat{G}^{ab}(\tau,\tau') = -i\left\langle T_C \hat{\Psi}(\tau_a) \otimes \hat{\Psi}^{+}(\tau'_b)\right\rangle, \tag{32}$$

where $a, b = +, -$ and T_C is the ordering operator at the Keldysh time contour which consists of the lower (superscript +) and upper (superscript −) parts (see Fig. 3).

In Eq. (32) the Nambu operator $\hat{\Psi}$ has the dimension $4(N + 4n) \times 1$. It means that it includes the Nambu operators for both SW and four NWs. In explicit form it reads:

$$\hat{\Psi} = \left(\hat{b}_{L1}...\hat{b}_{Ln}\hat{d}_{L1}...\hat{d}_{Ln}\hat{a}_1...\hat{a}_N\hat{b}_{R1}...\hat{b}_{Rn}\hat{d}_{R1}...\hat{d}_{Rn}\right)^T. \tag{33}$$

The steady current of the left lead is written as:

$$I = e\left\langle \dot{N}_L \right\rangle, \tag{34}$$

where $N_L = \sum_{k\sigma} c^{+}_{Lk\sigma} c_{Lk\sigma}$ is the operator of the particle number in the left contact. The solution of the Heisenberg equation yields for the current:

$$I = 2e \sum_k Tr\left[\hat{\sigma} Re\left\{\hat{t}^{+}_1(t)\hat{G}^{+-}_{k,L1}(t,t) + \hat{t}^{+}_n(t)\hat{G}^{+-}_{k,Ln}(t,t)\right\}\right], \tag{35}$$

where we put $\hbar = 1$. Note that in Eq. (35) we introduce the diagonal matrix $\hat{\sigma} = \mathrm{diag}(1, -1, 1, -1)$. In the same time,

$$\hat{t}_{1,n} = \frac{t_{1,2}}{2}\mathrm{diag}\left(e^{-i\frac{eVt}{2}}, e^{i\frac{eVt}{2}}, e^{-i\frac{eVt}{2}}, e^{i\frac{eVt}{2}}\right) \cdot \hat{\sigma} \tag{36}$$

are the diagonal matrices which depend on the time as a result of the unitary transformation of Rogovin and Scalapino [27]. Note that Rogovin-Scalapino transformation explicitly takes the bias voltage into account and reads:

$$\hat{U} = \exp\left\{\frac{ieVt}{2}\left(n_{Rk\sigma} - n_{Lk\sigma}\right)\right\}. \tag{37}$$

Performing this transformation transfers the voltage dependence into the interaction operator $\hat{V}$. Note that the linear time dependence in the exponents of $\hat{t}_{1,n}$ can be understood also from the nonequilibrium condition on the electrochemical potentials of the left and right contacts in the presence of the voltage according to Eq. (29).

Finally, in Eq. (35) for the current:

$$\hat{G}^{+-}_{k,L1} = i\left\langle \hat{b}^{+}_{L1} \otimes \hat{c}_{Lk}\right\rangle, \quad \hat{G}^{+-}_{k,Ln} = i\left\langle \hat{d}^{+}_{Ln} \otimes \hat{c}_{Lk}\right\rangle. \tag{38}$$

are the mixed Green's functions in Keldysh NEGF terminology.

It is important to stress that in the space of the Nambu operators the Hamiltonian of the device $\hat{H}_D$ has the form corresponding to the free particles. That is why in the averages entering in the definitions of the mixed Green's functions in Eq. (38) we should use the same prescriptions as for the averages in the T_C-ordered product of the secondly quantized operators [28, 29].

As a result, at $t \to 0$ Eq. (35) for the current can be written as:

$$I = 2e \int_C d\tau_1 Tr\Big[\hat{\sigma} Re\Big\{ \hat{\Sigma}^{+a}_{L1,L1}(-\tau_1)\hat{G}^{a-}_{L1,L1}(\tau_1) + \hat{\Sigma}^{+a}_{Ln,Ln}(-\tau_1)\hat{G}^{a-}_{Ln,Ln}(\tau_1) + \hat{\Sigma}^{+a}_{L1,Ln}(-\tau_1)\hat{G}^{a-}_{Ln,L1}(\tau_1) + \hat{\Sigma}^{+a}_{Ln,L1}(-\tau_1)\hat{G}^{a-}_{L1,Ln}(\tau_1) \Big\}\Big], \tag{39}$$

where

$$\hat{\Sigma}^{+a}_{Li,Lj}(-\tau_1) = \hat{t}^{+}_{i}(0)\hat{g}^{+a}_{Lk}(-\tau_1)\hat{t}_j(\tau_1) \tag{40}$$

are the self-energies of the left contact, $(i, j = 1, n)$, and $\hat{g}^{+a}_{Lk}(-\tau_1)$ is the bare Green's function of the left contact.

Integrating over the time τ and making the Fourier transform we finally get:

$$I = e \sum_{i,j=1,n} \int_{-\infty}^{+\infty} \frac{d\omega}{\pi} Tr\Big[\hat{\sigma} Re\Big\{ \hat{\Sigma}^{r}_{Li,Lj}(\omega)\hat{G}^{+-}_{Lj,Li}(\omega) + \hat{\Sigma}^{+-}_{Li,Lj}(\omega)\hat{G}^{a}_{Lj,Li}(\omega) \Big\}\Big], \tag{41}$$

where $\hat{\Sigma}^{r}_{Lj,Li}$ and $\hat{G}^{a}_{Lj,Li}$ are the block matrices of the retarded self-energies and advanced Green's functions respectively.

In principle it is possible to perform the further transformation of the Eq. (41) and obtain the explicit expression for the current which contains the terms corresponding to the local Andreev reflection and to the nonlocal transfer of the charge carriers. However, for the sake of simplicity we will not present these lengthy equations in this section.

Note that the real many-particle interactions are absent in the system which we consider here. That is why the self-energies and full Green's functions in Eqs. (40), (41) are determined taking into account all the tunneling processes between the device and the contacts. Correspondingly the block matrices $\hat{G}^{a}_{Lj,Li}$ of the advanced Green's functions of the whole device $\hat{G}^{a}$ are determined by the following Dyson equation:

$$\hat{G}^{a} = \Big[\big(\omega - \hat{h}_D - \hat{\Sigma}^{r}(\omega)\big)^{-1}\Big]^{+}, \tag{42}$$

where $\hat{h}_D$ is the Bogoliubov-de-Gennes matrix of the device Hamiltonian ($\hat{H}_D$) and $\hat{\Sigma}^{r}$ is the matrix of the retarded self-energy. It is frequency-dependent in general case and describes the effect of both contacts on the AB ring.

However, in our numerical calculations we will use more simple approximation of the wide-band contacts. In this approximation we can neglect the real parts of the self-energies and assume the imaginary parts to be constant [28, 29]. Then, we get the following explicit expressions for the nonzero blocks of the retarded self-energy $\hat{\Sigma}^{r}$:

$$\begin{aligned}\hat{\Sigma}^r_{L1,L1} =&\hat{\Sigma}^r_{Rn,Rn} = -\frac{i}{2}\hat{\Gamma}_{11}, \hat{\Sigma}^r_{R1,R1} = \hat{\Sigma}^r_{Ln,Ln} = -\frac{i}{2}\hat{\Gamma}_{22},\\ \hat{\Sigma}^r_{L1,Ln} =&\hat{\Sigma}^r_{R1,Rn} = \hat{\Sigma}^r_{Ln,L1} = \hat{\Sigma}^r_{Rn,R1} = -\frac{i}{2}\hat{\Gamma}_{12},\end{aligned} \tag{43}$$

In Eq. (43) we introduced the matrices:

$$\hat{\Gamma}_{ii} = \Gamma_i \hat{I}_4, \tag{44}$$

where $\hat{I}_4$ is 4×4 identity matrix,and

$$\Gamma_i = 2\pi t_i^2 \rho, \tag{45}$$

are the functions describing the broadening of the energy levels of the device related to its interaction with the ith contact. Finally, ρ in Eq. (45) is the density of states in the contact. In the expressions for the self -energies (43), off-diagonal broadenings are $\Gamma_{12} = \sqrt{\Gamma_1 \Gamma_2}$.

For the symmetric AB ring we will assume in the numerical calculations that $\Gamma_1 = \Gamma_2 = 0.01$. For the asymmetric ring we put $\Gamma_2 = \Gamma_1/2 = 0.01$. Then, assuming for simplicity that $\rho = 1/W$, where $W = 4t$—a bandwidth, one can obtain for the asymmetric configuration $t_1 \approx 0.11, t_2 \approx 0.08$.

The blocks $\hat{G}^{+-}_{Lj,Li}$ in the Eq. (41) for the current are governed by the solution of the Keldysh equation:

$$\hat{G}^{+-} = \hat{G}^r \hat{\Sigma}^{+-} \hat{G}^a, \tag{46}$$

Let us emphasize that we consider the regime where all the transition processes have been finished and thus the bare Green's functions of the device $\hat{g}$ do not enter in the Eq. (46) [29].

The nonzero blocks for the self-energies $\hat{\Sigma}^{+-}$ in Eq. (46) have the form

$$\hat{\Sigma}^{+-}_{\alpha i,\alpha j} = -2\hat{\Sigma}^r_{\alpha i,\alpha j}\hat{F}_\alpha, \tag{47}$$

where $\alpha = L, R, i, j = 1, n$; and we introduced the diagonal 4×4 matrix:

$$\hat{F}_{L(R)} = \mathrm{diag}\Big(n(\omega \pm eV/2),\ n(\omega \mp eV/2),\ n(\omega \pm eV/2),\ n(\omega \mp eV/2)\Big), \tag{48}$$

Note that $n(\omega \pm eV/2)$ in Eq. (48) are the Fermi-Dirac distribution functions.

6 Results of Numerical Calculations

In this section we present the results of the numerical calculations for the quantum transport. We will work in the regime of the linear response (small bias voltages) and consider the limit of low temperatures ($eV \to 0, k_B T \to 0$) for our system which consists of the device and contacts in Fig. 1.

We will start by considering the limiting case of the AB ring with the minimal number of sites. To be more specific we consider the case of six sites when $n = 1$ and $N = 2$. In Fig. 4a we show the dependence of the first 4 excitation energies E_{1-4} on the gate-field energy ϵ_d. Each color corresponds to the different excitation energy, i.e. 1st is red, 2nd is blue, 3rd is magenta and 4th is cyan. Due to degeneracy, curves of the same style (dotted, dashed, or solid) but different colors may overlap each other. In particular, at zero values of the Zeeman energy and Rashba constant $h = \alpha = 0$ the four states are splitted in energy on the two pairs of the doubly degenerate states (see the dotted curves in Fig. 4a).

Moreover, since in the general case the superconducting pairing in the ring is inhomogeneous, the gap Δ appears in the system at $\epsilon_d \neq 0$. However at zero gate field the energies $E_{1-4} = 0$, and that is why the differential conductance $G = dI/dV$

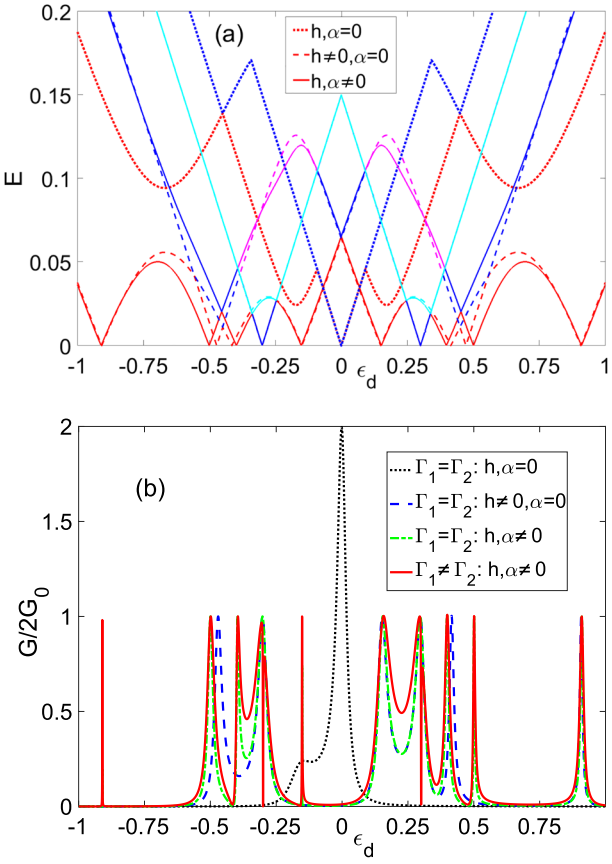

Fig. 4 The dependence of the excitation energies E_{1-4} (4a) and the conductance (4b) of the AB ring on the gate field ϵ_d. In the calculations we use the parameters: $n = 1$, $N = 2$ for the ring consisting of 6 sites, the hopping integral between NW and SW $t_0 = 0.5$, the Zeeman energy $h = 0.3$. We scale all the parameters in the units of the hopping integral $t = 1$ between the nearest neighbor sites in the SW

exhibits the $4G_0$ resonance peak, where $G_0 = e^2/h$ is the conductance quantum, only at $\epsilon_d = 0$ (see the dotted line in Fig. 4b).

The nonzero Zeeman energy leads to the gap suppression. As a result, the set of E_{1-4} zeros appears symmetrically relative to $\epsilon_d = 0$ as it is displayed by dashed curves in Fig. 4a. However not all the zeroes in the excitation energies manifest themselves as the resonances in the conductance. The reason for that is the formation of the bound states in the continuum (BICs). There are several possibilities to obtain the finite lifetime of this states.

One of the possibilities is to break the spatial symmetry of the eigenstates of the ring. It can be achieved e. g. by introducing the spin-orbit coupling in the system [30]. In this case the zeroes of the excitation spectrum related to the SW are slightly shifted (see the solid curves in Fig. 4a) and Fano resonances emerge in the conductance whose width is proportional to α (compare the dashed and dash-dotted curves in Fig. 4b at $\epsilon_d \approx \pm 0.4$). If $\alpha \ll t$ that there are couples of resonances, one of them is wide symmetric (of Breit-Wigner type) and another is narrow asymmetric (of Fano type). In double quantum dots emergence of such resonant patterns was interpreted as a manifestation of Dicke effect [31–33]. This phenomenon is known from optics and is expressed in the appearance of wide and narrow peaks in the luminescence spectrum of a pair of atoms [34–36]. The former is associated with a short-lived collective excitation (superradiant state), and the latter is with a long-lived one (subradiant state). Thus, we can conclude that the combination of the spin-orbit coupling and the external magnetic field (the Zeeman energy) allows to get the Dicke effect in the symmetric ring with the SC central region.

Let us emphasize that the zero-energy states at the values of the gate fields $\epsilon_d = \pm h$ remain doubly degenerate even at nonzero values of the Rashba constant $\alpha \neq 0$. This degeneracy is also connected with the symmetry of the AB-ring and leads to the emergence of the additional BICs [37, 38]. Their appearance can be observed in the conductance if we consider the asymmetric case for the tunneling parameters between the device and the contacts, $\Gamma_1 \neq \Gamma_2$. In this case the additional Fano resonances appear at $\epsilon_d = \pm h$ (see the solid curve in Fig. 4b). The similar effect is realized if we take into account the Aharonov–Bohm phase (see [39]).

Let us consider now the AB-ring with larger number of sites, namely we assume the parameters $n = 20$ and $N = 30$ for the NW and SW, respectively. According to [4, 6], in the nontrivial topological phase of the SW, when the set of inequalities (25) is fulfilled, and the Rashba constant $\alpha \neq 0$, we get the topological Dicke effect that is a set of couples of wide Breit-Wigner and narrow Fano resonances of the conductance.

Interesting features in the conductance related to the nonlocality of the MS appear in the asymmetric AB-ring. In this case we observe a set of additional narrow Fano resonances akin to the effect discussed above for the six-site system. One of such peaks appearing near the wide anti-resonance at $h \approx 1.22$ in Fig. 5a is shown in higher resolution in Fig. 5b by dashed curve.

We should stress, that when the length of the SC bridge (i.e. the SW length) is increased, the wide anti-resonance moves closer to the narrow Fano peak. Simultaneously, the narrow Fano peak collapses (its width goes to zero) and the BIC appears. We can clearly see this behavior in Fig. 5b. In other words, we can describe

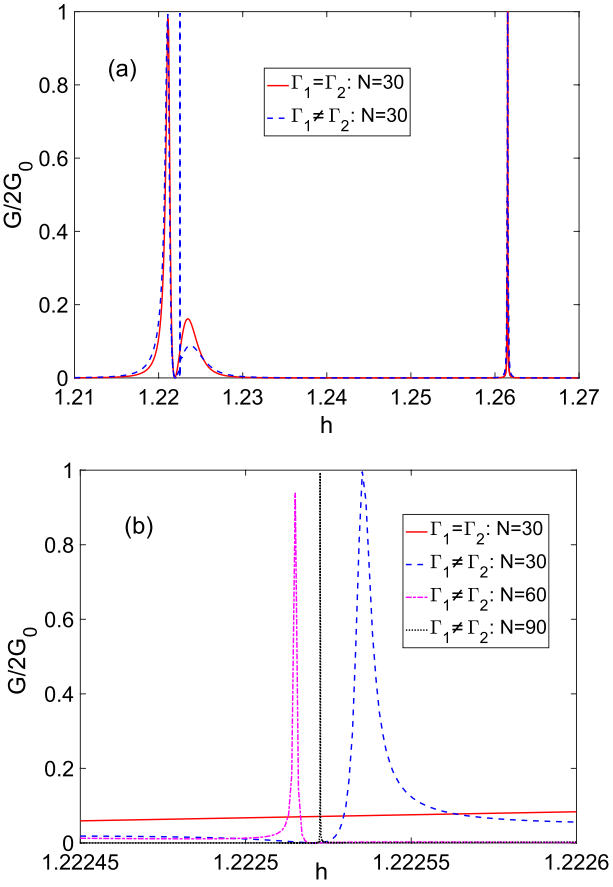

Fig. 5 Evolution of narrow Fano resonance related to the transport asymmetry in the AB ring. In Fig. 5a we show the pair of resonances (one is Fano resonance at $h \approx 1.22$, another one is Breit-Wigner resonance at $h \approx 1.26$) which appear in the conductance of the symmetric AB-ring as a function of the Zeeman energy. Note that in the asymmetric case ($\Gamma_1 \neq \Gamma_2$) a new narrow Fano peak occurs at $h \approx 1.22$. (5b) Collapse of the narrow Fano resonance with the strengthening of the MBS nonlocality controlled by N. The width of the Fano resonance depends crucially on the degree of the localization of the Majorana states in the SW. This fact makes it possible to use this effect for the detection of the Majorana excitations. The parameters are $n = 20$, $N = 30$, $t_0 = 0.1$ and $\epsilon_d = 1$

this situation as an unusual topological blockade of the Fano effect related to the asymmetry of the transport parameters of the ring. Indeed, the narrow Fano resonance disappears due to the nonlocality of the low-energy excitation in the SW.

To understand more deeply the mechanism which governs the collapse of the Fano resonance, it is important to note that this resonance is related to the BIC emerging due to the degeneracy of the zero-energy eigenstates of the closed system. Therefore, we can assume that the disappearance of the Fano resonance can be

explained by an increase in the multiplicity of the degeneracy of these states when the overlap of the Majorana wave-functions becomes negligible.

7 Toy Model Illustrating Collapse of Fano Resonance

To test our suggestion concerning the BIC formation caused by the MBS nonlocality, let us consider a spinless toy model for the AB-ring with $n = 1$ for the NW and $N = 2$ for the SW (see Fig. 2a). In other words, we can effectively consider the model of the Kitaev chain [12] with the even number of sites in the SC bridge.

In this situation the Hamiltonian of the AB-ring at the zero values $\epsilon_d = \mu = 0$ for the gate field and the chemical potential has the form:

$$H_D = \sum_{j=1}^{N-1} \left(-ta_j^+ a_{j+1} + \Delta a_j^+ a_{j+1}^+\right) - t_0 a_1^+ \left(b_{Ln} + b_{Rn}\right) - t_0 a_N^+ \left(d_{L1} + d_{R1}\right) + h.c. \tag{49}$$

Diagonalizing the Hamiltonian in Eq. (49), we get the following equation for the excitation spectrum:

$$\begin{aligned} &E^4 \left(E \cdot P_1 - 2t_0^2 \delta_1^{N/2-1}\right)\left(E \cdot P_2 + 2t_0^2 \delta_1^{N/2-1}\right) \cdot \\ &\cdot \left(E \cdot P_3 - 2t_0^2 \delta_2^{N/2-1}\right)\left(E \cdot P_4 + 2t_0^2 \delta_2^{N/2-1}\right) = 0, \end{aligned} \tag{50}$$

where $\delta_{1,2} = t \mp \Delta$ and $P_{i=1,\ldots,4}$ are the polynomials of the power $N/2$ with the property $P_{2,4} = P_{1,3}(E \to -E)$, which is connected with the electron–hole symmetry.

From the Eq. (50) it follows that for a special point of the Kitaev model [12], namely for $\Delta = \pm t$, the wave-functions of the Majorana fermions do not overlap, which was already mentioned in Sect. 3. Moreover, at this point the multiplicity of the degeneracy of the zero-energy states increases for $N > 2$, leading to the suppression of the narrow Fano resonance in Fig. 5b.

To develop these arguments further we again, as in Sect. 3, consider our system in the Majorana representation introducing self-conjugated Majorana operators $\gamma_{ij} = \gamma_{ij}^+$, $i = 1, 2$, which are connected with the fermionic operators via the relation $a_j = \left(\gamma_{1j} + i\gamma_{2j}\right)/2$.

In Figs. 2a and b in the framework of our description we present the sketch of the device corresponding to the special point of the Kitaev model $\Delta = t$ for the two cases of $N = 2$ (Fig. 2a) and $N > 2$ (Fig. 2b), respectively. The straight lines on these figures denote the interaction between the Majorana fermions of different sorts. We can see that for $N = 2$ on Fig. 2a the upper and lower shoulders of the device remain connected due to the absence of the SC pairing in the horizontal direction. Analysis of the eigenstate problem leads to a fourfold degeneracy of the excitation with zero energy [4].

However, for $N > 2$ on Fig. 2b the device is effectively divided into identical upper and lower subsystems. Each of the subsystems includes two chains of the

interacting quasi-particles. The simple estimates yield for the eigen-energies of the chains with only two bonds in the horizontal direction:

$$E_1 = 0, E_{2,3} = \pm t_0/\sqrt{2}, \tag{51}$$

If we include the vertical bond in the consideration practically in the same way as in the Fano-Anderson model [9, 40], then the eigen-energies read:

$$E_{1,2} = 0, E_{3,4} = \pm\sqrt{t^2 + t_0^2/2}, \tag{52}$$

Therefore, the degeneracy of the zero-energy state increases by two. Thus, we can say that it is just the appearance of the T-shaped structures of the Majorana fermions, which leads to the collapse of the Fano resonance in the asymmetric AB-ring.

Let us emphasize that the MBS nonlocality does not depend on the relationship between the tunneling parameters into the subsystems. Thus, the effect of the Fano resonance collapse has universal character and manifests itself in a more general situation, e.g., when these parameters are different from each other or a phase is added to t_0. According to Fig. 2 we observe, that the Fano resonance is not suppressed in the case of two noninteracting shoulders, i.e. when $t = 0$. We should stress, that the Fano resonance which we describe here in principle does not emerge in the symmetric case.

8 Fano Resonances in Local Transport Scheme

Finally, let us consider a limiting case of the above transport scheme by leaving only the left half of the system. In other words, in this section we turn to a Π-shaped device consisting of the LT and LB normal wires separated by the SW [41, 42].

Here to allow the wave functions of the MMs to leak out of the SW [43] and couple with the single contact, we suppose that the on-site energies in the NWs, $\xi_{1,2} = -\mu$, are lesser than the SW's one, $\xi = \epsilon_d - \mu$. In Fig. 6a a typical h-dependence of the linear-response conductance is displayed for the symmetric half ring, where h is satisfied the inequalities (25). One can observe both Breit-Wigner (symmetric) and Fano (asymmetric) resonances. It is important that the wide and narrow Fano peaks appear simultaneously even if $\Gamma_1 = \Gamma_2$ (see dashed curve). Moreover, the transport asymmetry ($\Gamma_1 \neq \Gamma_2$) does not induce new Fano resonances as it is depicted by solid curve. Remarkably, the wide and narrow peaks do not collapse if the SW length rises as it is shown in Fig. 6b. Obviously, one can see from the Figs. 2a and b that without the right-side-coupled quantum dots (i.e. the RT and RB normal wires with $n = 1$) there are no zero-energy states if $N = 2$. In turn, two such states occur if $N > 2$, one in each arm. At first glance it might seem that this is enough to obtain BIC here. However, as it was shown in [41], the presence of fundamental $\pi/2$-phase shift for tunneling into the MMs of different type prevents the BIC formation if the magnetic flux piercing the device plane (i.e. nonzero AB phase) is absent. Indeed, adapting the results of [41] for our case gives the following conductance expression at $|\omega| < \Delta$ (ω is a carrier energy):

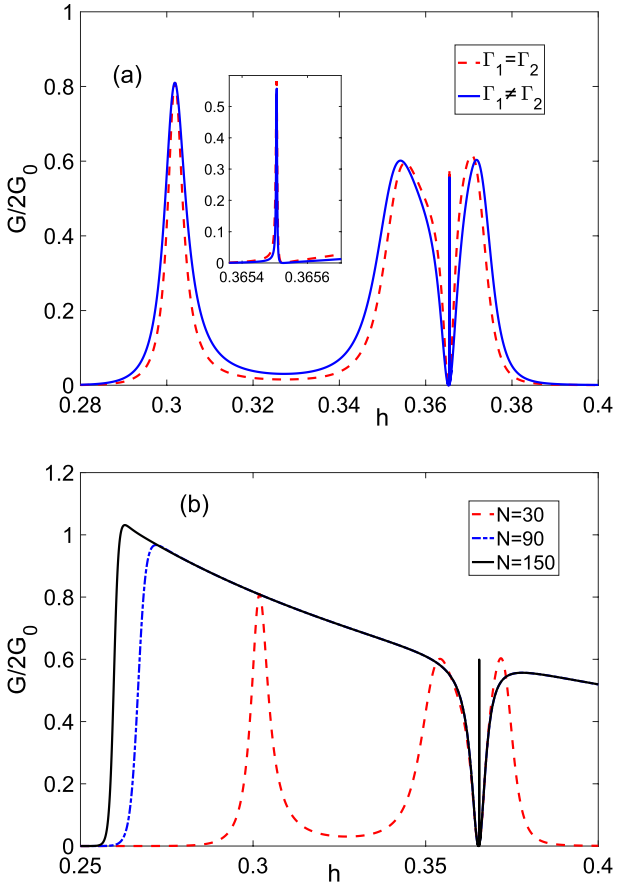

Fig. 6 Fano resonances in transport properties of the Π-shaped device with the superconducting bridge in the topologically nontrivial phase. **a** Linear-response conductance as a function of the Zeeman energy in the symmetric (dashed) and asymmetric (solid) transport regimes. Inset: persistence of the narrow Fano peak under the change in the transport symmetry. **b** h-dependencies of the conductance for the different bridge lengths. Note that the wide and narrow antiresonances are stable against the N change. The parameters are $n = 20$, $N = 30$, $t_0 = 0.1$ and $\epsilon_d = 1$

$$G = 2G_0 \cdot T_{\mathrm{LAR}},\ T_{\mathrm{LAR}} = 4t^4 t_0^4 D^2 \omega^2 \left[\Gamma_1^2 + \Gamma_2^2 - 2\Gamma_1\Gamma_2 \cos 2\phi\right] / \mid Z \mid^2, \quad (53)$$

where $D = C\left(\omega^2 - t_0^2\right) - t_0^2\left(\omega^2 - t_0^2\right)$,

$Z = Z_1 Z_2 + \frac{\Gamma_{12}^2}{4}\left(2z_1 z_2 + \omega^2 C^2 \frac{\Gamma_{12}^2}{4} - 8t^4 t_0^4 \cos 2\phi\right)$,

$Z_{1,2} = \omega\left(CC_{1,2}^2 + t_0^4\right) - 2t_0^2(C + 2t^2)C_{1,2}$, $z_{1,2} = C\left(\omega C_{1,2} - t_0^2\right) - 2t^2 t_0^2$,

$C = \omega^2 - 4t^2$, $C_{1,2} = \omega + i\Gamma_{1,2}/2$; ϕ is the AB phase. The in-gap conductance in the scheme with single normal contact is determined exclusively by processes of Local Andreev Reflection (LAR) [13, 44]. Hence, the factor 2 in the expression for G accounts for both electrons and holes. Now it is easy to realize that in the linear-response regime ($\omega = 0$) the antiresonance $G = 0$ occurs for any nonzero t_0, $\Gamma_{1,2}$ and

$\phi \neq \pi(n+1/2)$, $n \in \mathbb{Z}$. If $\phi = \pi(n+1/2)$, $n \in \mathbb{Z}$, the Green's function has a first-order pole at $\omega = 0$, i.e. $Z = \omega\tilde{Z}$. Then, the antiresonance collapses and $G = 2G_0$. In other words, $\omega = 0$ becomes a BIC energy.

9 Conclusion

Let us summarize the results presented in this article. We considered the asymmetric AB ring with different tunneling parameters. The shoulders of the ring are connected with the SC bridge in the topologically nontrivial phase. In this case the additional narrow Fano resonance emerges in the system due to the transport symmetry breaking. However, when we increase the length of the SC bridge, or in other words strongly reduce the overlap between the Majorana wave functions, this Fano resonance collapses.

To illustrate this effect, we studied the toy model of the spinless AB ring where the Kitaev chain serves as the SC bridge. The simple analytical estimates for the excitation spectrum of this model show the increase in the multiplicity of the degeneracy of the zero-energy state for the special point $\Delta = t$ of the Kitaev model at $N > 2$. The increase in the multiplicity is due to the formation of the T-shaped chains of the Majorana operators which leads to the appearance of the bound state in the continuum. Thus, we can conclude that the collapse of the resonance is a direct consequence of the MBS nonlocality [7, 45].

The additional study of the particular case of only half of the interferometer (i.e., when superconducting bridge on Fig. 1 is connected only to the left normal wires [41, 42]) demonstrated the persistence of the stability of the Fano peaks when transport symmetry changes (from symmetric to asymmetric). Using the spinless toy model it is shown that the fundamental $\pi/2$-phase shift for tunneling into the MMs of different type prevents the collapse of Fano resonances and BIC emergence.

The performed analysis allows to propose a way to probe the MBS nonlocality, based on the properties of Fano resonances. First, in the parametric region corresponding to the topologically nontrivial phase of the SW, one should look for the narrow Fano peaks emerging when the transport scheme becomes asymmetric (the tunnel parameters $t_{1,2}$ can be controlled in experiment by gate electrodes). Second, the in-plane magnetic field or supergate [21], placed along the bridge area, can be utilized to control the overlap of the MMs wave functions by varying the Zeeman energy or on-site energy in the SW, respectively [46]. As a result, if the overlap tends to zero the narrow Fano resonances have to collapse. Third, when the local transport geometry is investigated (it can be achieved by employing gate electrodes to eliminate coupling of the SW with, e.g., the RT and RB normal leads) the narrow Fano peaks should be robust to the transport mode switching.

Acknowledgements We were inspired by Andreev's seminal contribution in the superconducting nanophysics—the field which started in fact from Josephson effect and Andreev reflection. M. Yu. Kagan thanks the Program for basic research of the National Research University Higher School of Economics for support. The work was partially carried out within the state assignment of Kirensky Institute of Physics. S.V.A. thanks the Foundation for the Advancement of Theoretical Physics and Mathematics "BASIS" for support.

References

1. E. Majorana II., Nuovo Cimento (1924-1942) **14**, 171 (2008)
2. A.Y. Kitaev, Ann. Phys. **303**, 2 (2003). https://doi.org/10.1016/S0003-4916(02)00018-0
3. S.R. Elliott, M. Franz, Rev. Mod. Phys. **87**, 137 (2015). https://doi.org/10.1103/RevModPhys.87.137
4. V.V. Valkov, M.S. Shustin, S.V. Aksenov, A.O. Zlotnikov, A.D. Fedoseev, V.A. Mitskan, M.Y. Kagan, Phys. Usp. **65**, 2 (2022). https://doi.org/10.3367/UFNe.2021.03.038950
5. Y. Aharonov, D. Bohm, Phys. Rev. **115**, 485 (1959). https://doi.org/10.1103/PhysRev.115.485
6. V.V. Val'kov, M.Y. Kagan, S.V. Aksenov, J. Phys.: Condens. Matter. **31**, 225301 (2019). https://doi.org/10.1088/1361-648X/ab0b8c
7. S.V. Aksenov, M.Y. Kagan, JETP Lett. **111**, 286 (2020). https://doi.org/10.1134/S0021364020050057
8. J. Neumann, F. Wigner, Phys. Z. **30**, 465 (1929)
9. U. Fano, Phys. Rev. **124**, 1866 (1961)
10. E.I. Rashba, V.I. Sheka, Fiz. Tverd. Tela **11**, 162 (1959)
11. Yu.A. Bychkov, E.I.R. Sov, Phys. JETP Lett. **39**, 78 (1984)
12. A.Y. Kitaev, Phys. Usp. **44**, 131 (2001). https://doi.org/10.1070/1063-7869/44/10S/S29
13. A.F. Andreev, Sov. Phys. JETP **19**, 1228 (1964)
14. A.F. Andreev, Sov. Phys. JETP **22**, 455 (1966)
15. J.-J. Xia, S.-Q. Duan, W. Zhang, Nanoscale Res. Lett. **10**, 223 (2015)
16. R.M. Lutchyn, J.D. Sau, S.D. Sarma, Phys. Rev. Lett. **105**, 077001 (2010). https://doi.org/10.1103/PhysRevLett.105.077001
17. Y. Oreg, G. Refael, F. Oppen, Phys. Rev. Lett. **105**, 177002 (2010). https://doi.org/10.1103/PhysRevLett.105.177002
18. V. Mourik, K. Zuo, S.M. Frolov, S.R. Plissard, E.P.A.M. Bakkers, L.P. Kouwenhoven, Science **336**, 1003 (2012). https://doi.org/10.1126/science.1222360
19. J. Alicea, Rep. Prog. Phys. **75**, 076501 (2012)
20. L. Fidkowski, R.M. Lutchyn, C. Nayak, M.P.A. Fisher, Phys. Rev. B **84**, 195436 (2011). https://doi.org/10.1103/PhysRevB.84.195436
21. R.M. Lutchyn, E.P.A.M. Bakkers, L.P. Kouwenhoven, P. Krogstrup, C.M. Marcus, Y. Oreg, Nat. Rev. Mat. **3**, 52 (2018). https://doi.org/10.1038/s41578-018-0003-1
22. S. Das Sarma, Nat. Phys. **19**, 165 (2023). https://doi.org/10.1038/s41567-022-01900-9
23. S.M. Frolov, P. Zhang, B. Zhang, Y. Jiang, S. Byard, S.R. Mudi, J. Chen, A.-H. Chen, M. Hocevar, M. Gupta, C. Riggert, V.S. Pribiag, Preprint at https://arxiv.org/abs/2309.09368 (2023)
24. V.V. Valkov, V.A. Mitskan, A.O. Zlotnikov, M.S. Shustin, S.V. Aksenov, JETP Lett. **110**, 140 (2019). https://doi.org/10.1134/S002136401914011X
25. L.V.J. Keldysh, Theor. Exp. Phys. **20**, 1018 (1965)
26. Y. Nambu, Phys. Rev. **117**, 648 (1960). https://doi.org/10.1103/PhysRev.117.648
27. D. Rogovin, D.J. Scalapino, Ann. Phys. (N.Y.) **86**, 1 (1974)
28. P.I. Arseev, N.S. Maslova, V.N. Mantsevich, JETP **115**, 141 (2012)
29. P.I. Arseev, Phys. Usp. **59**, 1159 (2015)
30. M.P. Nowak, B. Szafran, F.M. Peeters, Phys. Rev. B **84**, 235319 (2011)
31. T.V. Shahbazyan, M.E. Raikh, Phys. Rev. B **49**, 17123 (1994)
32. T. Vorrath, T. Brandes, Phys. Rev. B **68**, 035309 (2003)
33. P.A. Orellana, M.L. Landron de Guevara, F. Claro, Phys. Rev. B **70**, 235315 (2004)
34. R.H. Dicke, Phys. Rev. **89**, 472 (1953)
35. R.H. Dicke, Phys. Rev. **93**, 99 (1954)
36. T. Brandes, Phys. Rep. **408**, 315 (2005)
37. A. Volya, V. Zelevinsky, Phys. Rev. C **67**, 054322 (2003)
38. A.F. Sadreev, E.N. Bulgakov, I. Rotter, Phys. Rev. B **73**, 235342 (2006)
39. H. Lu, R. Lu, B.-F. Zhu, Phys. Rev. B **71**, 235320 (2005). https://doi.org/10.1103/PhysRevB.71.235320
40. P.W. Anderson, J. Phys. C **3**, 2436 (1970)
41. S.V. Aksenov, J. Phys.: Condens. Matter. **34**, 255301 (2022). https://doi.org/10.1088/1361-648X/ac62a7
42. S.V. Aksenov, Phys. Rev. B **107**, 085417 (2023). https://doi.org/10.1103/PhysRevB.107.085417

43. E. Vernek, P.H. Penteado, A.C. Seridonio, J.C. Egues, Phys. Rev. B **89**, 165314 (2014). https://doi.org/10.1103/PhysRevB.89.165314
44. V.V. Val'kov, S.V.J. Aksenov, Magn. Magn. Mat. **465**, 88 (2018). https://doi.org/10.1016/j.jmmm.2018.04.043
45. M.Y. Kagan, S.V. Aksenov, A.V. Turlapov, R.S. Ikhsanov, K.I. Kugel, E.A. Mazur, E.A. Kuznetsov, V.M. Silkin, E.A. Burovskii, JETP Lett. **117**, 755 (2023)
46. Das Sarma, S. Sau, J.D. Stanescu, T.D. Phys, Rev. B **86**, 220506(R) (2012). https://doi.org/10.1103/PhysRevB.86.220506